RL-TR-96-239
In-House Report
March 1997

ADAPTIVE CFAR DETECTION AND REDUCED-RANK SPACE-TIME ADAPTIVE PROCESSING

J. Scott Goldstein, Capt., USAF
Irving S. Reed (Advisor,Univ. of Southern California)

APPROVED FOR PUBLIC RELEASE; DISTRIBUTION UNLIMITED.

Rome Laboratory
Air Force Materiel Command
Rome, New York

This report has been reviewed by the Rome Laboratory Public Affairs Office (PA) and is releasable to the National Technical Information Service (NTIS). At NTIS it will be releasable to the general public, including foreign nations.

RL-TR-96-239 has been reviewed and is approved for publication.

APPROVED: 

DANIEL J. MCAULIFFE
Chief, Communications Division
Command, Control & Communications Directorate

FOR THE COMMANDER: 

JOHN A. GRANIERO, Chief Scientist
Command, Control & Communications Directorate

If your address has changed or if you wish to be removed from the Rome Laboratory mailing list, or if the addressee is no longer employed by your organization, please notify Rome Laboratory/C3BA, Rome, NY 13441. This will assist us in maintaining a current mailing list.

Do not return copies of this report unless contractual obligations or notices on a specific document require that it be returned.

REPORT DOCUMENTATION PAGE

Form Approved
OMB No. 0704-0188

1. AGENCY USE ONLY (Leave Blank)	2. REPORT DATE	3. REPORT TYPE AND DATES COVERED
	March 1997	In-House

4. TITLE AND SUBTITLE
ADAPTIVE CFAR DETECTION AND REDUCED-RANK SPACE-TIME ADAPTIVE PROCESSING

5. FUNDING NUMBERS
PE - 64479F
PR - 4056
TA - 00
WU - 02

6. AUTHOR(S)
J.Scott Goldstein, Capt., USAF
Irving S. Reed (Advisor, Univ. of Southern California)

7. PERFORMING ORGANIZATION NAME(S) AND ADDRESS(ES)
Rome Laboratory/C3BA
525 Brooks Road
Rome, NY 13441-4505

8. PERFORMING ORGANIZATION REPORT NUMBER

9. SPONSORING/MONITORING AGENCY NAME(S) AND ADDRESS(ES)
Rome Laboratory/C3BA
525 Brooks Road
Rome, NY 13441-4505

10. SPONSORING/MONITORING AGENCY REPORT NUMBER
RL-TR-96-239

11. SUPPLEMENTARY NOTES
Rome Laboratory Project Engineer: J. Scott Goldstein, Capt., USAF, RL/C3BA, (315)330-7316.

12a. DISTRIBUTION/AVAILABILITY STATEMENT
Approved for public release; distribution unlimited.

12b. DISTRIBUTION CODE

13. ABSTRACT (Maximum 200 words)

A new approach to adaptive CFAR detection and reduced-rank space-time adaptive processing is introduced. A general methodology is developed for the design and analysis of reduced-rank detectors with known and unknown covariance. The detection and false alarm probabilities are explicitly calculated and a cross-spectral metric is introduced for rank reduction. This metric is demonstrated to result in a low-rank detector which outperforms the principal components technique. The cross-spectral metric provides subspace dimensionality robustness and allows for the dimension of the detector to be reduced beneath the dimension of the noise subspace eigenstructure without significant performance loss.

14. SUBJECT TERMS
detection theory, CFAR detection, space-time adaptive processing, rank reduction, partially adaptive sensor array processing

15. NUMBER OF PAGES
56

16. PRICE CODE

17. SECURITY CLASSIFICATION OF REPORT	18. SECURITY CLASSIFICATION OF THIS PAGE	19. SECURITY CLASSIFICATION OF ABSTRACT	20. LIMITATION OF ABSTRACT
UNCLASSIFIED	UNCLASSIFIED	UNCLASSIFIED	U/L

Contents

List of Figures

1 Introduction

This report is concerned with optimal space-time adaptive processing (STAP) in environments which cannot support fully-adaptive processing due to either size, weight, and power restrictions or sample support limitations. Typical sensor platforms which exhibit such restrictions include those that operate in airborne, space-segment, and undersea environments. The primary difficulty in STAP is that the dimension of the adaptive weight vector, which equals the product of the number of antenna elements and the number of Doppler bins, becomes large. Both the required sample support for STAP detection and the computational complexity of the algorithms, which update this weight vector, increase in proportion to the dimension of the weight vector. When the data from auxillary range gates are used for interference and clutter estimates, the required large sample support necessitates the use of range gates which are relatively far from the range gate of interest. These distant range gates may not preserve the homogeneity of the clutter and may not provide good estimates of the interference near the range gate of interest, thereby resulting in degraded performance.

Thus, real-time STAP implementations need a lower rank processor to be realizable from a computational viewpoint. A dilemma is encountered when the optimal steady-state solution requires a larger number of weights than the platform can support. In this report a general methodology is developed which reduces the dimensionality of the weight vector for target detection without adversely affecting the steady-state solution.

The optimal weight vector for adaptive signal detection takes the form of a linearly constrained Wiener filter [1, 2, 3, 4, 5, 6, 7], where the constraint is in angle and Doppler. It is noted that this linear constraint is not the same as the popular minimum-variance, distortionless-response

(MVDR) constraint for wideband arrays [8]. At first glance the form of the constrained Wiener filter for STAP and target detection does not provide much insight to the rank-reduction problem. As a consequence there is no clear methodology for finding the conditions needed to optimize a partially adaptive STAP system.

The most effective previously proposed reduced-rank solutions to the STAP problem require an eigendecomposition of the array covariance matrix or its estimate [9, 10, 11, 12, 13, 14, 15]. These methods are based on the principal component approximation of a covariance matrix [16, 17]. One goal of approximating the covariance matrix with a low-rank estimate is to simplify the weight update algorithm. Notably, the weight vector obtained by reducing the rank of the covariance matrix through the use of the principal components technique has full dimension [12, 13, 14, 15]. Finally, the principal component approach requires that the dimension of the noise subspace eigenstructure be known precisely. This dimension corresponds to the true rank of the interference-plus-clutter covariance matrix. Since this rank is never known a priori, it must be estimated. The penalty for underestimating the rank of this total noise contribution can be great; the detection performance degrades rapidly as the rank of the detector is decreased below the dimension of the noise subspace eigenstructure.

In this report a new method is introduced to achieve a reduced-rank array processor using what is called a cross-spectral metric. This metric was introduced recently for narrowband MVDR processors and least squares adaptive filters [18, 19]. For these cases the cross-spectral metric is shown to provide an upper-bound on the minimum mean-square error performance obtainable by all other eigen-based techniques. In this report the use of the cross-spectral metric is extended to STAP for target detection. It is shown that this metric also maximizes the output signal-to-interference plus noise ratio (SINR) [6, 20], thereby optimizing the weight vector for signal detection

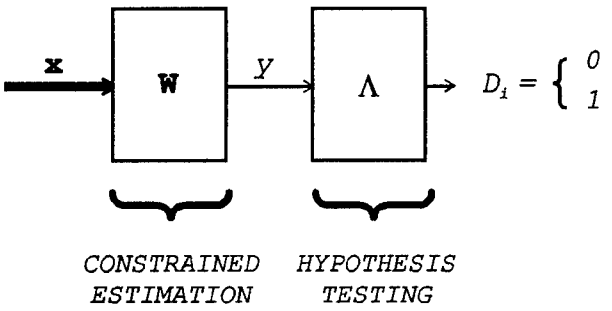

Figure 1: The Optimal Joint Gaussian Detector.

under the joint Gaussian assumption [3].

The optimal processor is partitioned by means of a unitary operator which results in a structure called the generalized sidelobe canceller (GSC) [2, 21]. The GSC processor results in both a lower dimensional weight vector and an unconstrained optimal filter. The GSC is the canonical processor for signal detection, and it is by means of this sidelobe canceller interpretation that the process of rank reduction is motivated. Since the cross-spectral metric results in the analytical optimization of the SINR as a function of the weight vector dimension, a reduced-rank weight vector is obtained which best preserves the steady-state performance.

The optimal processor for detection under the joint Gaussian assumption is interpreted as consisting of two systems in cascade, as depicted in Figure 1. The first system is a noise field estimator which utilizes the constrained Wiener filter. This estimation system produces the best estimate of the test cell with which the presence or absence of a target is to be determined. The second system consists of a hypothesis testing mechanism which implements the detection criterion. The input to the optimal processor is the observed radar return, and the output is a decision D_i with respect to target presence ($D_i = 1$) or absence ($D_i = 0$). With this interpretation of the optimal detector, the process of partial adaptivity belongs within the first system, and results in reduced-rank estimation.

The space-time adaptive processing framework is developed in Sect. 2. In Sect. 3 the detection criterion termed an AMF CFAR test is reviewed with a known covariance in terms of the standard direct-form detector. The equivalent full-rank GSC detector is derived in Sect. 4. The GSC form processor is utilized next in Sect. 5 to derive a new reduced-rank GSC AMF CFAR detector which uses the cross-spectral metric. Here it is demonstrated that the cross-spectral metric maximizes the output SINR as a function of the rank of the processor. The statistics of the reduced-rank AMF CFAR test with known and unknown covariance are derived in Sect. 6. An example of the performance of partially adaptive STAP for target detection is presented in Sect. 7, and the conclusions are provided in Sect. 8.

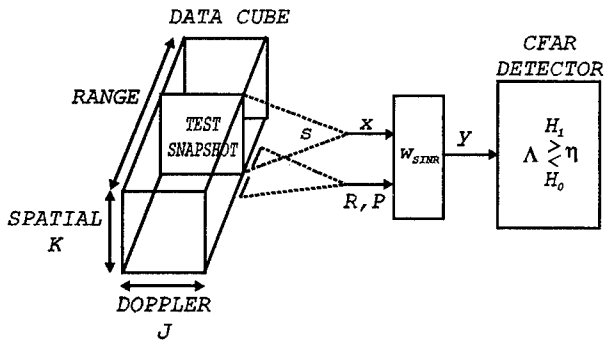

Figure 2: 3-dimensional CPI data cube.

2 Space-Time Adaptive Processing

Radar returns are collected in a coherent processing interval (CPI), which may be represented as the 3-D data cube shown in Figure 2. The data is then processed at one range of interest, which corresponds to a slice of the CPI data cube. This slice is a $J \times K$ space-time snapshot, denoted by $\mathbf{X}$. This space-time snapshot can be expressed also as the matrix

$$\mathbf{X} = \begin{bmatrix} x_{0,0} & x_{0,1} & \cdots & x_{0,K-1} \\ x_{1,0} & x_{1,1} & \cdots & x_{1,K-1} \\ \vdots & \vdots & \ddots & \vdots \\ x_{J-1,0} & x_{J-1,1} & \cdots & x_{J-1,K-1} \end{bmatrix}, \tag{1}$$

where the individual elements $x_{\mathrm{j,k}}$ correspond to the data from the j-th pulse repetition interval (PRI) and the k-th sensor element [3, 22].

The 2-D space-time data structure consists of element space information and PRI space-Doppler information. If a target is present in the range gate of interest, then the return $\mathbf{X}$ is composed of components due to the target, the interference sources or jammers, clutter, and white noise:

$$\mathbf{X} = \mathbf{X}_t + \mathbf{X}_i + \mathbf{X}_c + \mathbf{X}_w. \tag{2}$$

If no target is present, then the snapshot consists only of interference, clutter and white noise. The white noise in the space-time snapshot is the thermal noise present at the sensor elements, which

is both spatially and temporally white. Each of the other components of the radar return are now addressed.

The target is assumed to approximate a point target, present in only one range gate. The $J \times K$ space-time snapshot corresponding to the target is then given by

$$\mathbf{X}_t = \alpha_t \mathbf{b}(\omega_t)\mathbf{a}^H(\vartheta_t), \tag{3}$$

where $\mathbf{a}(\vartheta_t)$ is the $K \times 1$ spatial steering vector in the direction provided by the target spatial frequency ϑ_t, $\mathbf{b}(\omega_t)$ is the $J \times 1$ temporal steering vector at the target Doppler frequency ω_t, and α_t is the amplitude of the target. The target data is then stacked column-wise to form the $KJ \times 1$ target vector

$$\mathbf{x}_t = \alpha_t \mathbf{b}(\omega_t) \otimes \mathbf{a}(\vartheta_t), \tag{4}$$

where $(\cdot) \otimes (\cdot)$ represents the Kronecker tensor product operator.

The interference environment consists of several sources which are assumed temporally to be white (barrage jammers spread over all Doppler frequencies at a particular azimuth). The $J \times K$ space-time snapshot corresponding to the jammers is given by

$$\mathbf{X}_i = \boldsymbol{\alpha}_i \mathbf{A}^H(\vartheta_i), \tag{5}$$

where $\boldsymbol{\alpha}_i$ is the $J \times I$ matrix of jammer amplitudes for the J PRI's of each of the I interference sources and $\mathbf{A}(\vartheta_i)$ is the $K \times I$ matrix whose i-th row is the spatial steering vector for the i-th interference source with spatial frequency ϑ_i. The interference data is stacked column-wise to form the $KJ \times 1$ interference vector $\mathbf{x}_i$.

The clutter returns are assumed to come from all areas within a common range gate in a direction towards which the antenna is directed. Consider returns from a circular ring about the

platform. If each spot within a clutter ring is a point-like reflector, its space-time snapshot takes the form,

$$\mathbf{X}_{c_p} = \alpha_{c_p}\mathbf{b}(\omega_{c_p})\mathbf{a}^H(\vartheta_{c_p}), \tag{6}$$

where ϑ_{c_p} and ω_{c_p} are the spatial and Doppler frequencies of the clutter return from the p-th patch, and α_{c_p} is the power from the p-th clutter patch. If the clutter is assumed to be locally stationary, it has a velocity relative to the radar platform which is determined by the azimuth angle between the array and the clutter patch. Finally, if the clutter returns are assumed to come from this clutter ring which is divided into a large number D of evenly spaced sectors and summed, the total return from the clutter has the form,

$$\mathbf{X}_c = \sum_{\phi_{c_p}=1}^{D} \alpha_{c_p}\mathbf{b}(\beta\vartheta_{c_p})\mathbf{a}^H(\vartheta_{c_p}), \tag{7}$$

where β is the constant of linearity between the spatial and Doppler frequencies. The spatial frequency is given by

$$\vartheta_{c_p} = \frac{d}{\lambda_o}\cos\theta_c \sin\phi_{c_p}, \tag{8}$$

with d, λ_o, and θ_c being the element spacing, wavelength, and fixed elevation angle, respectively. The clutter data is then stacked column-wise to form the $KJ \times 1$ vector $\mathbf{x}_c$.

The total input noise vector $\mathbf{n}$ is given by

$$\mathbf{n} = \mathbf{x}_i + \mathbf{x}_c + \mathbf{x}_w. \tag{9}$$

The input noise covariance matrix is then defined to be

$$\mathbf{R} = \mathbf{E}\left[\mathbf{n}\mathbf{n}^H\right]. \tag{10}$$

3 The AMF CFAR Test with Known Covariance

Radar detection is a binary hypothesis problem, where hypothesis H_1 corresponds to target presence and hypothesis H_0 corresponds to target absence. Each of the components of the space-time snapshot vector $\mathbf{x}$ are assumed to be independent, complex, multivariate Gaussian. This snapshot, for each of the two hypothesis, is of the form,

$$\begin{array}{ll} H_0: & \mathbf{x} = \mathbf{n}, \\ H_1: & \mathbf{x} = \mathbf{x}_t + \mathbf{n}. \end{array} \tag{11}$$

The $KJ \times 1$-dimensional space-time steering vector $\mathbf{v}(\vartheta_t, \omega_t)$ is defined as follows:

$$\mathbf{v}(\vartheta_t, \omega_t) = \mathbf{b}(\omega_t) \otimes \mathbf{a}(\vartheta_t), \tag{12}$$

where $\mathbf{b}(\omega_t)$ and $\mathbf{a}(\vartheta_t)$ are introduced in (3). For convenience in the analysis to follow, the normalized steering vector in the space-time look-direction is defined to be

$$\mathbf{s} = \frac{\mathbf{v}(\vartheta_t, \omega_t)}{\sqrt{\mathbf{v}^H(\vartheta_t, \omega_t)\mathbf{v}(\vartheta_t, \omega_t)}}. \tag{13}$$

The normalized target gain α is then given by

$$\alpha = \alpha_t \sqrt{\mathbf{v}^H(\vartheta_t, \omega_t)\mathbf{v}(\vartheta_t, \omega_t)}, \tag{14}$$

where the original target gain α_t is introduced in (3). The two hypothesis in (11) may now be written in the form

$$\begin{array}{ll} H_0: & \mathbf{x} = \mathbf{n}, \\ H_1: & \mathbf{x} = \alpha\mathbf{s} + \mathbf{n}, \end{array} \tag{15}$$

where $\alpha = |\alpha| e^{j\phi}$ is a complex gain whose random phase ϕ is uniformly distributed between 0 and 2π. The random vector $\mathbf{x}$, when conditioned on ϕ, is Gaussian under both hypotheses. The conditional probability densities of $\mathbf{x}$ are

$$\begin{aligned} f_{x|H_1,\phi}(\mathbf{x}) &= \frac{1}{\pi^{KJ}||\mathbf{R}||} e^{-(\mathbf{x}-\alpha\mathbf{s})^H \mathbf{R}^{-1}(\mathbf{x}-\alpha\mathbf{s})}, \\ f_{x|H_0,\phi}(\mathbf{x}) &= \frac{1}{\pi^{KJ}||\mathbf{R}||} e^{-\mathbf{x}^H \mathbf{R}^{-1}\mathbf{x}}, \end{aligned} \tag{16}$$

where $||(\cdot)||$ is the determinant operator. The likelihood ratio test then takes the form,

$$\Lambda = \frac{f_{x|H_1}(\mathbf{x})}{f_{x|H_0}(\mathbf{x})} = \frac{\frac{1}{2\pi}\int_0^{2\pi} f_{x|H_1,\phi}(\mathbf{x})d\phi}{\frac{1}{2\pi}\int_0^{2\pi} f_{x|H_0,\phi}(\mathbf{x})d\phi} \underset{H_0}{\overset{H_1}{\gtrless}} \eta, \tag{17}$$

where η is some threshold. Using the densities in (16), the test in (17) becomes

$$\Lambda = \mathbf{I}_o\left(2|\alpha|\left|\mathbf{s}^H\mathbf{R}^{-1}\mathbf{x}\right|\right) e^{-|\alpha|^2\mathbf{s}^H\mathbf{R}^{-1}\mathbf{s}} \underset{H_0}{\overset{H_1}{\gtrless}} \eta, \tag{18}$$

where $\mathbf{I}_o(\cdot)$ is the modified Bessel function of the first kind. The noise covariance matrix $\mathbf{R}$ is nonnegative definite and the modified Bessel function is monotonically increasing in its argument. Therefore, the test in (18) reduces to

$$\Lambda_1 = \left|\mathbf{s}^H\mathbf{R}^{-1}\mathbf{x}\right|^2 \underset{H_0}{\overset{H_1}{\gtrless}} \eta_1, \tag{19}$$

where the new threshold η_1 is related to the previous threshold η as follows:

$$\eta_1 = \left[\frac{\mathbf{I}_o^{-1}\left(\eta e^{|\alpha|^2\mathbf{s}^H\mathbf{R}^{-1}\mathbf{s}}\right)}{2|\alpha|}\right]^2. \tag{20}$$

The test in (19) was the STAP detection criterion, developed in the well known papers by Brennan and Reed [3] and Reed, Mallett and Brennan (RMB) [4]. The RMB test takes the form of a matched filter for incoherent detection and is a Bayes optimal test which is maximally invariant with respect to the group of phase shifts. However, as noted by Kelly [23], no predetermined threshold can be set to achieve a specified false alarm probability since the detector is designed to operate in an unknown interference environment.

The RMB test in (19) can be modified to have a constant false alarm rate (CFAR) property via a normalization by the output power. This new test, derived independently in [24] and [25], is termed an adaptive matched filter (AMF). The AMF CFAR test takes the form,

$$\Lambda_2 = \frac{\left|\mathbf{s}^H\mathbf{R}^{-1}\mathbf{x}\right|^2}{\mathbf{s}^H\mathbf{R}^{-1}\mathbf{s}} \underset{H_0}{\overset{H_1}{\gtrless}} \eta_2, \tag{21}$$

and is an optimum group invariant hypothesis test with respect to the change-of-scale and the initial target phase groups. The probability of detection for the AMF CFAR test Λ_2 is given by [24]

$$P_D = \sum_{n=0}^{\infty} \left(\frac{\xi^n e^{-\xi}}{n!} \right) Q\left(n+1, \eta_2\right), \tag{22}$$

where ξ is the output signal-to-interference plus noise ratio, $Q\left(\cdot\right)$ is the incomplete gamma function, and the threshold η_2 is found from the false alarm probability:

$$P_{FA} = Q\left(1, \eta_2\right) = e^{-\eta_2}. \tag{23}$$

The RMB and AMF CFAR tests may be interpreted as functions of an optimal weight vector $\mathbf{w}_{\text{SINR}}$ [4], which is obtained by an unconstrained optimization of the SINR as follows:

$$\mathbf{w}_{\text{SINR}} = k\mathbf{R}^{-1}\mathbf{s}, \tag{24}$$

where k is some arbitrary complex constant. The constrained optimization implemented by the sidelobe canceller form, which is introduced in the next section, fixes the value of k to provide a normalization by the output power. The weight vector in (24) is now considered using a constrained optimization for target detection under the joint Gaussian assumption. The optimal constrained weight vector for maximizing the output SINR, while maintaining a normalized response in the target spatio-Doppler look-direction, was originally given in [2] as follows:

$$\mathbf{w}_{\text{SINR}} = \frac{\mathbf{R}^{-1}\mathbf{s}}{\mathbf{s}^H\mathbf{R}^{-1}\mathbf{s}}. \tag{25}$$

The output y formed by applying this latter weight vector to the primary data is

$$y = \mathbf{w}_{\text{SINR}}^H\mathbf{x} = \frac{\mathbf{s}^H\mathbf{R}^{-1}\mathbf{x}}{\mathbf{s}^H\mathbf{R}^{-1}\mathbf{s}}, \tag{26}$$

and the resulting output SINR is

$$\xi = \frac{|\alpha|^2}{P} = \frac{|\alpha|^2}{\mathbf{w}_{\text{SINR}}^H\mathbf{R}\mathbf{w}_{\text{SINR}}} = |\alpha|^2\mathbf{s}^H\mathbf{R}^{-1}\mathbf{s}, \tag{27}$$

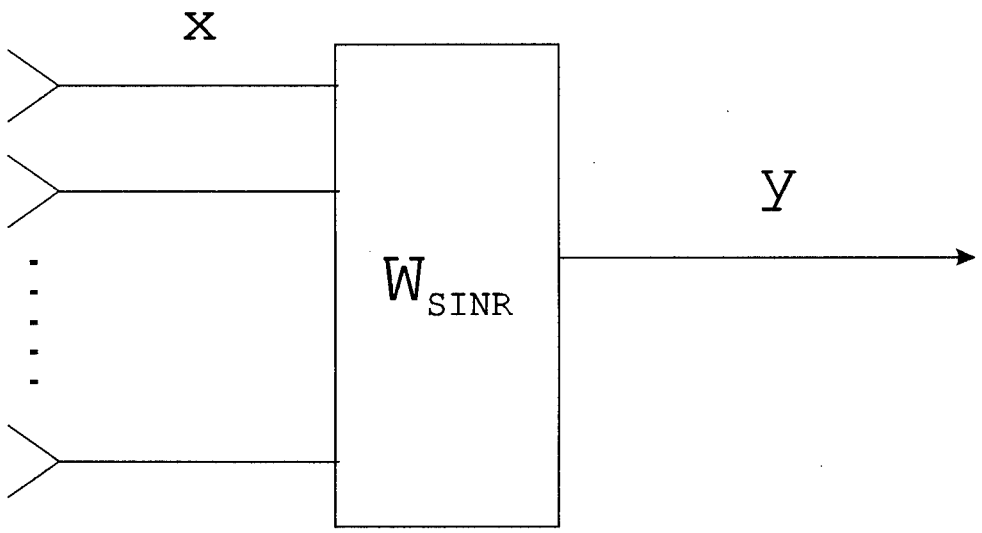

Figure 3: The direct-form processor.

where $|\alpha|^2$ is the output power due to the target signal under hypothesis H_1 and

$$P = \frac{1}{\mathbf{s}^H \mathbf{R}^{-1} \mathbf{s}} \tag{28}$$

is the output noise power of the processor. The weight vector in (25) is the result of a constrained optimization in which a beam is placed in that spatial and Doppler look-direction which is given by the steering vector $\mathbf{s}$. This direct-form processor is depicted in Figure 3.

The RMB test in (19) may now be expressed in the form

$$\Lambda_1 = \left(\mathbf{s}^H \mathbf{R}^{-1} \mathbf{s}\right)^2 |y|^2 = \left|\frac{y}{P}\right|^2 \underset{H_0}{\overset{H_1}{\gtrless}} \eta_1, \tag{29}$$

which demonstrates that the RMB detector compares a threshold η_1 with the ratio of the output power to the square of the noise output power. The normalized AMF test in (21) may similarly be written in the form,

$$\Lambda_2 = \left(\mathbf{s}^H \mathbf{R}^{-1} \mathbf{s}\right) |y|^2 = \frac{|y|^2}{P} \underset{H_0}{\overset{H_1}{\gtrless}} \eta_2, \tag{30}$$

where the threshold η_2 is now compared with the ratio of the output power to the noise output power.

An equivalent new AMF CFAR detector is now developed which is characterized by a sidelobe canceller form. This sidelobe canceller form is used next to reduce the dimension of the weight vector $\mathbf{w}_{\text{SINR}}$, which maximizes the output SINR and the probability of detection under the joint Gaussian assumption. The goal of this data reduction step is to obtain a reduced-dimensional test criterion which yields decisions which correspond with the full-dimensional AMF CFAR test in (21).

4 The GSC Form Processor

The direct-form STAP processor described in Sect. 3 is now transformed into the generalized sidelobe canceller (GSC) form. The GSC processor results in an unconstrained weight vector and reformulates the STAP detector structure into the form of a standard Wiener filter. This GSC form of the detector provides a deeper insight to the rank-reduction problem than appears to be possible otherwise.

Consider now using a unitary $KJ \times KJ$ matrix operator $\mathbf{T}$ to transform the data prior to adaptive detection. The unitary nature of this matrix conserves power, so that the resulting output SINR is seen to be identical to the original direct-form detection processor. The structure of this operator is partitioned as follows:

$$\mathbf{T} = \begin{bmatrix} \mathbf{s}^H \\ \mathbf{B} \end{bmatrix}, \tag{31}$$

where the $KJ \times 1$-dimensional conventional space-time beamformer $\mathbf{s}$ is defined in (13) and $\mathbf{B}$ is the full-row rank $N \times KJ$ signal blocking matrix which maps $\mathbf{x}$ onto the null-space of $\mathbf{s}$, where $N = (KJ - 1)$. Hence,

$$\mathbf{Bs} = \mathbf{0}, \tag{32}$$

so that the matrix $\mathbf{B}$ effectively blocks any signal coming from the spatio-Doppler look-direction. Any full row-rank matrix $\mathbf{B}$ that satisfies (32) and results in an invertible $\mathbf{T}$ is a valid signal blocking matrix. The Gram-Schmidt algorithm may be applied then to this matrix to generate an orthonormal $\mathbf{B}$ and a unitary $\mathbf{T}$. Two algorithms for directly finding an orthonormal $\mathbf{B}$, using the singular value decomposition (SVD) and the QR decomposition, respectively, are described in Appendix A.

The transformation of the radar return $\mathbf{x}$ by the operator $\mathbf{T}$ in (31) yields a vector $\tilde{\mathbf{x}}$ which has

the form

$$\tilde{\mathbf{x}} = \mathbf{T}\mathbf{x} = \begin{bmatrix} \mathbf{s}^H\mathbf{x} \\ \mathbf{B}\mathbf{x} \end{bmatrix} = \begin{bmatrix} d \\ \mathbf{b} \end{bmatrix}, \tag{33}$$

where the scalar-valued beamformed output is denoted by d. Here also the N-dimensional vector $\mathbf{b}$ is termed the noise subspace data vector. It is seen now that the transformed data vector $\tilde{\mathbf{x}}$ has an associated covariance matrix $\mathbf{R}_{\tilde{x}}$ which takes the form:

$$\mathbf{R}_{\tilde{x}} = \mathbf{T}\mathbf{R}\mathbf{T}^H = \begin{bmatrix} \sigma_d^2 & \mathbf{r}_{bd}^H \\ \mathbf{r}_{bd} & \mathbf{R}_b \end{bmatrix}. \tag{34}$$

The $N \times N$ noise subspace covariance matrix $\mathbf{R}_b$ is expressed by

$$\mathbf{R}_b = \mathbf{E}[\mathbf{b}\mathbf{b}^H] = \mathbf{B}\mathbf{R}\mathbf{B}^H. \tag{35}$$

The $N \times 1$ cross-correlation vector between the noise subspace data vector and the beamformer output is given by

$$\mathbf{r}_{bd} = \mathbf{E}[\mathbf{b}d^*] = \mathbf{B}\mathbf{R}\mathbf{s}, \tag{36}$$

where $*$ represents the complex conjugate operator. The scalar σ_d^2 in (34) is computed to be

$$\sigma_d^2 = \mathbf{s}^H\mathbf{R}\mathbf{s}, \tag{37}$$

and represents the variance of the conventional beamformer output.

Next let $\mathbf{T}$ operate on the steering vector $\mathbf{s}$. This operation yields the unit transformed, steering vector $\mathbf{e}_1$, given by

$$\mathbf{e}_1 = \mathbf{T}\mathbf{s} = \begin{bmatrix} 1 \\ 0 \\ \vdots \\ 0 \end{bmatrix}. \tag{38}$$

Then the optimal weight vector in these transformed coordinates is given by

$$\mathbf{w}_{gsc} = \frac{\mathbf{R}_{\tilde{x}}^{-1}\mathbf{e}_1}{\mathbf{e}_1^H\mathbf{R}_{\tilde{x}}\mathbf{e}_1} = \begin{bmatrix} 1 \\ -\mathbf{w} \end{bmatrix}, \tag{39}$$

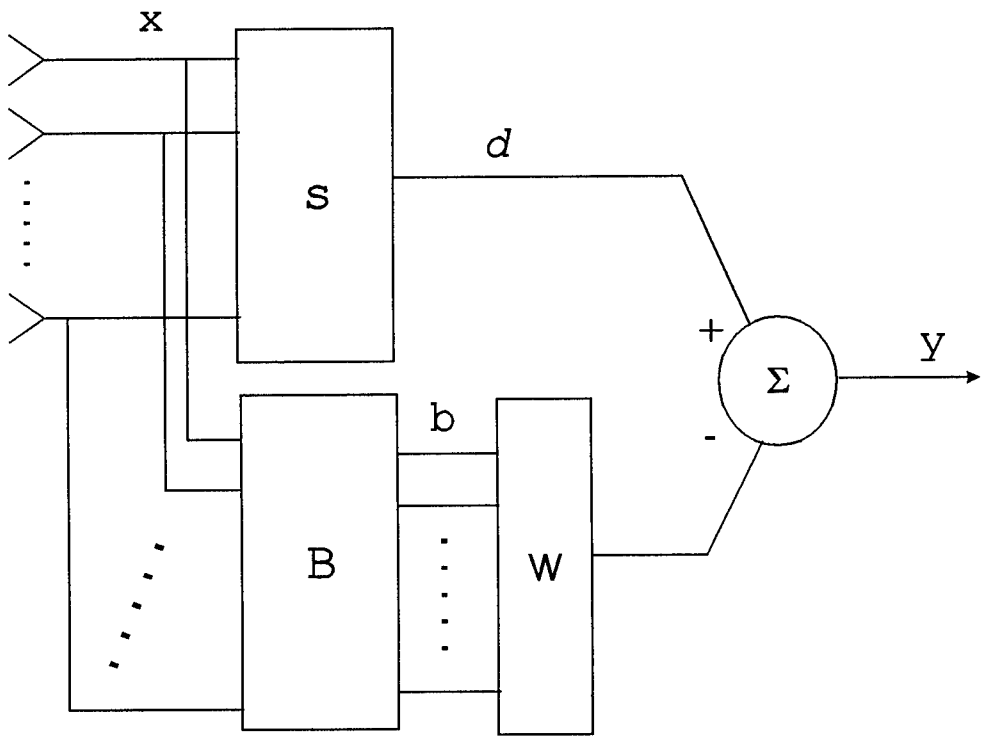

Figure 4: The full-rank GSC processor.

where $\mathbf{R}_{\tilde{x}}$ is the covariance matrix in (34). The partitioning of the matrix operator $\mathbf{T}$ leads naturally to the form of the GSC array processor depicted in Figure 4 [2, 7, 21]. This processor results in a fixed weight of unity for the upper branch and an adaptive weight vector $\mathbf{w}$ of dimension $N = KJ-1$ in the lower branch. The vector $\mathbf{w}$ in (39) is provided by the Wiener solution corresponding to the filter depicted in Figure 4:

$$\mathbf{w} = \mathbf{R}_b^{-1}\mathbf{r}_{bd}, \tag{40}$$

where $\mathbf{R}_b$ and $\mathbf{r}_{bd}$ are computed in (35) and (36), respectively. The GSC form processor implements the KJ-dimensional weight vector in (39) using the partitioning defined in (33). The steady-state performance of the GSC and the direct-form processor are identical, but the adaptive weight vector $\mathbf{w}$ in the GSC is of a lower dimension. Hence, the computational requirements for updating this weight vector are reduced and the GSC form therefore can be considered canonical.

The output of the arrays, utilizing the weight vectors described in (25) and (39), are identical and, using (33) and (39), may be expressed as follows:

$$y = \mathbf{w}_{SINR}^H \mathbf{x} = \mathbf{w}_{gsc}^H \tilde{\mathbf{x}} = \left(\mathbf{s}^H - \mathbf{w}^H \mathbf{B}\right) \mathbf{x}. \tag{41}$$

The output noise power is found by a substitution of (40) into (41) and the evaluation of the mean-square value of y using (28) as follows:

$$P = \frac{1}{\mathbf{s}^H \mathbf{R}^{-1} \mathbf{s}} = \sigma_d^2 - \mathbf{r}_{bd}^H \mathbf{R}_b^{-1} \mathbf{r}_{bd}. \tag{42}$$

The definitions of the filters $\mathbf{s}$ and $\mathbf{B}$ imply that the output SINR may be written by (27) in a more illuminating form as follows:

$$\xi = \frac{|\alpha|^2}{\sigma_d^2 - \mathbf{r}_{bd}^H \mathbf{R}_b^{-1} \mathbf{r}_{bd}}. \tag{43}$$

The observation data covariance matrix $\mathbf{R}_b$ is expressed now in terms of its eigenvectors and eigenvalues as follows:

$$\mathbf{R}_b = \mathbf{U} \boldsymbol{\Lambda} \mathbf{U}^H, \tag{44}$$

where $\mathbf{U}$ is a unitary $N \times N$ matrix composed of the eigenvectors $\{\boldsymbol{\mathcal{V}}_i\}_{i=1}^N$ and $\boldsymbol{\Lambda}$ is the diagonal matrix of associated eigenvalues $\{\lambda_i\}_{i=1}^N$. The noise process $\mathbf{b}$, defined implicitly in (33) is transformed to a principal coordinate process $\mathbf{p}$ as follows:

$$\mathbf{p} = \mathbf{U}^H \mathbf{b}. \tag{45}$$

A normal component covariance matrix $\mathbf{R}_p$, cross-correlation vector $\mathbf{r}_{pd}$, and Wiener filter $\mathbf{w}_N$ are defined now as follows:

$$\mathbf{R}_p = \mathbf{E}[\mathbf{p}\mathbf{p}^H] = \mathbf{U}^H \mathbf{R}_b \mathbf{U} = \boldsymbol{\Lambda}, \tag{46}$$

$$\mathbf{r}_{pd} = \mathbf{E}[\mathbf{p} d^*] = \mathbf{U}^H \mathbf{r}_{bd}, \tag{47}$$

$$\mathbf{w}_N = \mathbf{R}_p^{-1} \mathbf{r}_{pd} = \mathbf{U}^H \mathbf{w}. \tag{48}$$

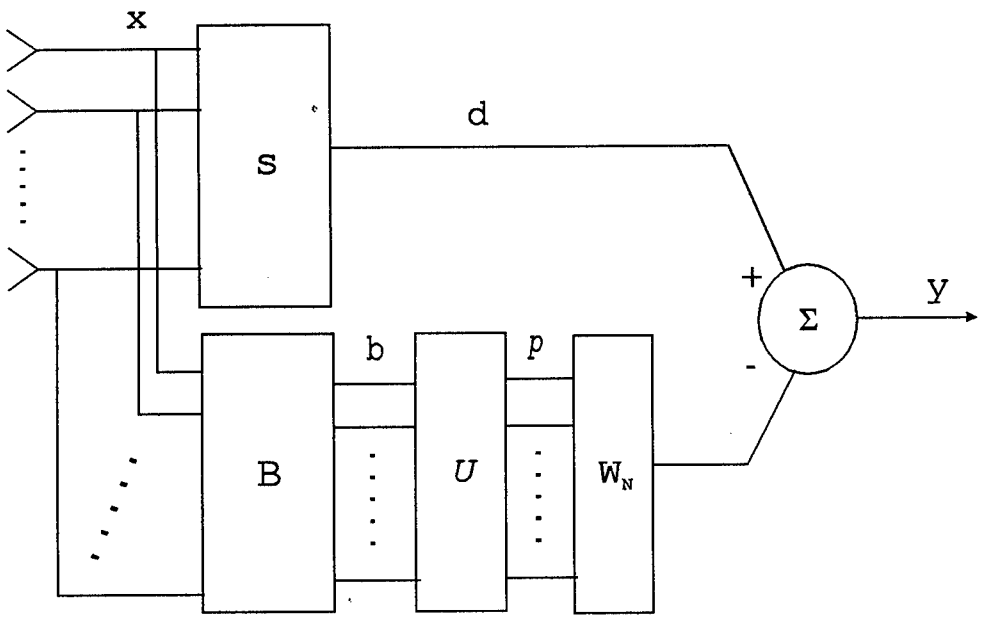

Figure 5: The full-rank GSC processor in principal coordinates.

The GSC in these normal coordinates, depicted in Figure 5, is equivalent to the GSC in Figure 4 in terms of its steady-state characteristics. The array output of the GSC in normal coordinates is given by

$$y = \left(\mathbf{s}^H - \mathbf{w}_N^H \mathbf{U}^H \mathbf{B}\right) \mathbf{x} = \left(\mathbf{s}^H - \mathbf{w}^H \mathbf{B}\right) \mathbf{x}. \tag{49}$$

Note that the output noise power,

$$P = \sigma_d^2 - \mathbf{r}_{pd}^H \mathbf{R}_p^{-1} \mathbf{r}_{pd} = \sigma_d^2 - \mathbf{r}_{bd}^H \mathbf{R}_b^{-1} \mathbf{r}_{bd}, \tag{50}$$

and that the SINR,

$$\xi = \frac{|\alpha|^2}{\sigma_d^2 - \mathbf{r}_{pd}^H \mathbf{R}_p^{-1} \mathbf{r}_{pd}} = \frac{|\alpha|^2}{\sigma_d^2 - \mathbf{r}_{bd}^H \mathbf{R}_b^{-1} \mathbf{r}_{bd}}, \tag{51}$$

are conserved by any unitary transformation, including that realized by the operator $\mathbf{U}$.

5 Partially Adaptive STAP and the Cross-Spectral Metric

We now derive the cross-spectral metric for optimal subspace selection and rank reduction in partially adaptive STAP. The problem of reducing the degrees of freedom for an array processor involves selecting a subset or some combination of the elements to be adaptively weighted. For notational purposes, let the space spanned by the columns of the fully adaptive array covariance matrix be denoted by $\mathcal{C}^N$, implying that the observation covariance matrices $\mathbf{R}_b$ and $\mathbf{R}_p$ are of dimension $N \times N$ and the vectors $\mathbf{r}_{bd}$, $\mathbf{r}_{pd}$, $\mathbf{w}$, and $\mathbf{w}_N$ are $N \times 1$-dimensional vectors. The partially adaptive GSC shown in Figure 6 utilizes an $N \times M$ transformation operator $\boldsymbol{\mathcal{U}}$, in place of $\mathbf{U}$ in Figure 5, to form the M-dimensional reduced-rank observation data vector,

$$\mathbf{z} = \boldsymbol{\mathcal{U}}^H \mathbf{b}, \tag{52}$$

where $M < N$. The associated $M \times M$ reduced-rank covariance matrix is given by

$$\mathbf{R}_z = \boldsymbol{\mathcal{U}}^H \mathbf{R}_b \boldsymbol{\mathcal{U}} = \boldsymbol{\Lambda}_M, \tag{53}$$

where $\boldsymbol{\Lambda}_M$ is the diagonal matrix composed of the M eigenvalues corresponding to the eigenvectors to be selected which form $\boldsymbol{\mathcal{U}}$. The cross-correlation between the process $\mathbf{z}$ and the desired signal d is given by

$$\mathbf{r}_{zd} = \mathbf{E}[\mathbf{z}d^*] = \boldsymbol{\mathcal{U}}^H \mathbf{r}_{bd}. \tag{54}$$

The data vector $\mathbf{z}$ is then processed by the reduced-rank weight vector $\mathbf{w}_M$, which is of dimension $M \times 1$. From Wiener filter theory this weight vector is expressed finally by

$$\mathbf{w}_M = \mathbf{R}_z^{-1} \mathbf{r}_{zd} = \boldsymbol{\Lambda}_M^{-1} \boldsymbol{\mathcal{U}}^H \mathbf{r}_{bd}. \tag{55}$$

The most popular technique for subspace selection is based on the principal components method [9, 11, 12, 13, 14]. This method determines the singular value decomposition of the $N \times N$-

dimensional covariance matrix $\mathbf{R}_b$ and selects the M largest eigenvectors (those corresponding to the largest eigenvalues) to form the M-dimensional eigen-subspace $\boldsymbol{\Psi} \subset \boldsymbol{\mathcal{C}}^N$ in which the adaptive processor operates. However, this technique does not directly consider the maximum output SINR performance measure to maximize the probability of detection, which is a function of not only the space spanned by the noise covariance matrix $\mathbf{R}_b$ but also of the cross-correlation between the desired signal d and the noise process $\mathbf{b}$.

The derivation in [18] is now used to reduce the rank of the Wiener filter in a manner which maximizes the output SINR. To accomplish this a rank reducing $N \times M$ transformation matrix $\boldsymbol{\mathcal{U}}$, which is composed of some M columns from $\mathbf{U}$, needs to be selected (see Figure 6). The operator $\boldsymbol{\mathcal{U}}$ is constrained therefore to be a subset of M of the N possible eigenvectors of $\mathbf{R}_b$. This particular constraint allows a direct comparison with the principal component technique, which chooses the rank reducing transform to be composed of those M eigenvectors which correspond to the largest M eigenvalues. Thus, the particular problem at hand is to choose the subspace spanned by a set of M eigenvectors out of the N available such that the resulting M-dimensional Wiener filter yields the largest output SINR out of all $\binom{N}{M}$ possible combinations of eigenvectors. The subspace spanned by the columns of the optimal reduced-rank covariance matrix which achieves this maximization of the output SINR as a function of filter rank is denoted by $\boldsymbol{\Omega} \subset \boldsymbol{\mathcal{C}}^N$.

Now denote the reduced-rank processor output by y_r. This is illustrated in Figure 6. A study of Figures 5 and 6 suggest that the reduced-rank processor output may be expressed by the relation,

$$y_r = \left[1, \quad \mathbf{w}_N^H \mathbf{U}^H - \mathbf{w}_M^H \boldsymbol{\mathcal{U}}^H\right] \begin{bmatrix} y \\ \mathbf{b} \end{bmatrix}. \tag{56}$$

Denote the weight error vector between the full-rank weight vector and its reduced-rank version by

$$\boldsymbol{\epsilon} = \mathbf{U}\mathbf{w}_N - \boldsymbol{\mathcal{U}}\mathbf{w}_M. \tag{57}$$

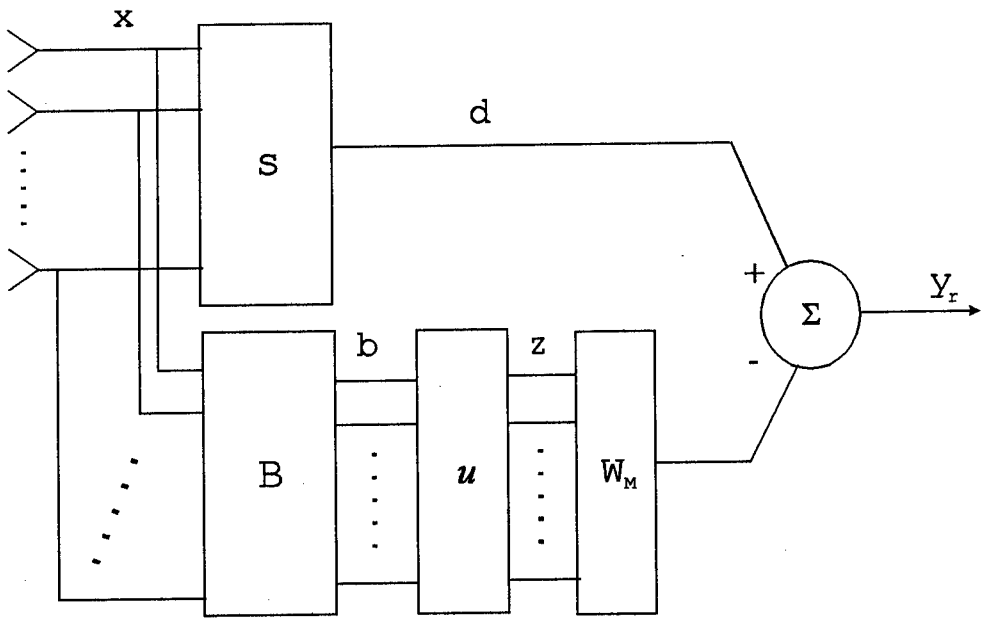

Figure 6: The reduced-rank GSC processor.

By (50) the output noise power for the reduced-rank processor is now computed in this notation to be

$$P_r = \sigma_d^2 - \mathbf{r}_{pd}^H \mathbf{R}_p^{-1} \mathbf{r}_{pd} + \epsilon^H \mathbf{R}_b \epsilon \geq P, \tag{58}$$

and the reduced-rank SINR is expressed as

$$\xi_r = \frac{|\alpha|^2}{\sigma_d^2 - \mathbf{r}_{pd} \mathbf{R}_p^{-1} \mathbf{r}_{pd} + \epsilon^H \mathbf{R}_b \epsilon} \leq \xi. \tag{59}$$

Note that the target signal power is not affected by rank reduction; the rank reduction is only a function of the noise field estimation. A comparison of (50) with (58) or (51) with (59), shows that it is desirable to choose the rank reducing operator $\boldsymbol{\mathcal{U}}$ in a manner that minimizes the additional mean-square error incurred by the rank reduction. Define the $N \times M$ subspace index matrix $\mathbf{J}$, given by

$$\mathbf{J} = \mathbf{U}^H \boldsymbol{\mathcal{U}}. \tag{60}$$

This matrix is composed of N orthonormal unit vectors and N-M null vectors in an order which

corresponds with the selection of the M columns of $\mathbf{U}$ that were retained to form the rank reducing operator $\boldsymbol{\mathcal{U}}$. Now, one wants to minimize the scalar term $\epsilon^H \mathbf{R}_b \epsilon$ which appears in (58) and (59) as follows:

$$\min\left[\epsilon^H \mathbf{R}_b \epsilon\right] = \min\left[\left(\mathbf{w}_N^H \mathbf{R}_p^{1/2} - \mathbf{w}_M^H \mathbf{R}_z^{1/2} \mathbf{J}^H\right)\left(\mathbf{R}_p^{1/2} \mathbf{w}_N - \mathbf{J}\mathbf{R}_z^{1/2} \mathbf{w}_M\right)\right]. \tag{61}$$

Thus evidently the best solution for (61) is to choose that set of M rows of $\mathbf{U}$ for the $M \times N$ matrix $\boldsymbol{\mathcal{U}}$ such that $\mathbf{J}\mathbf{R}_z^{1/2}\mathbf{w}_M$ is the best low rank approximation to the vector $\mathbf{R}_p^{1/2}\mathbf{w}_N$.

The Wiener-Hopf relationship for the full-rank case is given by

$$\mathbf{R}_p \mathbf{w}_N = \mathbf{r}_{pd}. \tag{62}$$

A multiplication of both sides of (62) by $\mathbf{R}_p^{-1/2}$ on the left yields the following relationships:

$$\begin{aligned} \mathbf{R}_p^{1/2}\mathbf{w}_N &= \mathbf{R}_p^{-1/2}\mathbf{r}_{pd} = \boldsymbol{\Lambda}^{-1/2}\mathbf{U}^H \mathbf{r}_{bd} \\ &= \begin{bmatrix} \frac{\boldsymbol{\mathcal{V}}_1^H \mathbf{r}_{bd}}{\sqrt{\lambda_1}} \\ \frac{\boldsymbol{\mathcal{V}}_2^H \mathbf{r}_{bd}}{\sqrt{\lambda_2}} \\ \vdots \\ \frac{\boldsymbol{\mathcal{V}}_N^H \mathbf{r}_{bd}}{\sqrt{\lambda_N}} \end{bmatrix}. \end{aligned} \tag{63}$$

Hence in order to make the vector $\mathbf{J}\mathbf{R}_z^{1/2}\mathbf{w}_M$ be the best low rank approximation to the vector $\mathbf{R}_p^{1/2}\mathbf{w}_N$, it is necessary to rank order the terms in (63) by their magnitude. With this ranking of the eigenvectors which compose the matrix $\mathbf{U}$, the index matrix $\mathbf{J}$ takes the form

$$\mathbf{J} = \begin{bmatrix} \mathbf{I} \\ \mathbf{0} \end{bmatrix}, \tag{64}$$

where $\mathbf{I}$ is the $M \times M$ identity matrix and $\mathbf{0}$ is the $(N - M) \times M$ null matrix. Then the rank reducing operator $\boldsymbol{\mathcal{U}}$ is selected by choosing those M eigenvectors of $\mathbf{U}$ which correspond with the largest M values of the sequence of non-negative terms

$$\left|\frac{\boldsymbol{\mathcal{V}}_i^H \mathbf{r}_{bd}}{\sqrt{\lambda_i}}\right|^2, \tag{65}$$

for $i = 1, 2, \ldots N$. Note that the metric in (65) measures the cross-spectral energy projected along the i-th eigenvector. With this selection, the columns of the reduced-rank covariance matrix $\mathbf{R}_z$ span the M-dimensional cross-spectral subspace $\boldsymbol{\Omega} \subset \mathcal{C}^N$ to provide the largest output SINR of any M-dimensional subspace which is spanned by M of the N columns of $\mathbf{U}$.

Clearly, the subspace $\boldsymbol{\Omega}$ spanned by the columns of eigenvectors corresponding with the M largest values of the cross-spectral metric is not the same as the subspace $\boldsymbol{\Psi}$ spanned by the eigenvectors corresponding with the M largest eigenvalues for all values of M. This means that the Wiener filter in the cross-spectral subspace $\boldsymbol{\Omega}$ yields an output SINR which is always larger than or equal to that provided by the Wiener filter in the subspace $\boldsymbol{\Psi}$. We conclude that the reduced-rank Wiener filter found via the cross-spectral metric maximizes the output SINR as a function of the rank of the filter for the eigenvector basis. Thus the cross-spectral metric results in an upper-bound on the performance of eigen-based rank reduction techniques.

To demonstrate that the cross-spectral metric is optimal for each rank $M \leq N$, we consider the decomposition of the SINR performed by the full-rank matrix of eigenvectors $\mathbf{U}$. The output SINR of the full-rank processor, from (46) and (51), can be expressed as

$$\xi = \frac{|\alpha|^2}{\sigma_d^2 - \sum_{i=1}^{N} \frac{\left|\boldsymbol{\nu}_i^H \mathbf{r}_{bd}\right|^2}{\lambda_i}}. \tag{66}$$

The optimal reduced-rank SINR is expressed as

$$\xi_r = \frac{|\alpha|^2}{\sigma_d^2 - \sum_{j \in \boldsymbol{\Omega}} \frac{\left|\boldsymbol{\nu}_j^H \mathbf{r}_{bd}\right|^2}{\lambda_j}}. \tag{67}$$

Finally, a comparison of the decision rule in (65) with the expressions in (66) and (67) demonstrate that the cross-spectral metric maximizes the output SINR as a function of the rank of the weight vector.

6 The Reduced-Rank AMF CFAR Test with Known and Unknown Convariance

The AMF CFAR test in (21) is defined in terms of the output signal y and the output noise power P of the direct form processor. The GSC is then derived as the canonical form of this optimal array processor in Sect. 4, where it is also demonstrated that the GSC yields an output signal and SINR which are equivalent with that provided by the direct-form processor.

An optimal reduced-rank STAP design technique is derived in Sect. 5, where the GSC form processor was utilized. It is also shown in Sect. 5 that the target signal power is not affected by rank reduction. Thus, as mentioned in Sect. 1, the process of rank reduction for partially adaptive STAP belongs within the noise field estimation system shown in Figure 1. The cross-spectral metric provides an upper-bound on the output SINR achievable by reduced-rank detectors using an eigenvector basis. This fact explains why the cross-spectral metric provides a capability to achieve reduction in the rank of the weight vector below the dimension of the noise subspace eigenstructure without a significant loss in performance. The cross-spectral metric given in (65) provides the best set of the possible $\binom{N}{M}$ eigenvectors of the noise subspace covariance matrix to select for rank reduction. These optimal eigenvectors are then used by the hypothesis testing mechanism to determine target presence or absence. A new optimal reduced-rank AMF CFAR test is now formally defined and analyzed.

For convenience, we now rewrite the AMF CFAR test in (30) as follows:

$$\Lambda_2 = \frac{\left|\mathbf{s}^H\mathbf{R}^{-1}\mathbf{x}\right|^2}{\mathbf{s}^H\mathbf{R}^{-1}\mathbf{s}} = \frac{|y|^2}{P} \underset{H_0}{\overset{H_1}{\gtrless}} \eta_2. \tag{68}$$

The reduced-rank array output y_r, derived in (56) and depicted in Figure 6, is written now in the

form,

$$y_r = \left(\mathbf{s}^H - \mathbf{w}_M^H \boldsymbol{\mathcal{U}}^H \mathbf{B}\right) \mathbf{x} = d - \mathbf{w}_M^H \mathbf{z} = d - \mathbf{r}_{zd}^H \mathbf{R}_z^{-1} \mathbf{z}. \tag{69}$$

Also the reduced-rank output noise power P_r in (58) may be expressed by

$$P_r = \sigma_d^2 - \mathbf{r}_{zd}^H \mathbf{R}_z^{-1} \mathbf{r}_{zd}, \tag{70}$$

where the covariance matrix $\mathbf{R}_z$ and the cross-correlation vector $\mathbf{r}_{zd}$ were defined in (53) and (54), respectively. In terms of the expressions in (69) and (70), a new optimal reduced-rank version of the AMF CFAR test is obtained as follows:

$$\Lambda_{2r} = \frac{|y_r|^2}{P_r} \underset{H_0}{\overset{H_1}{\gtrless}} \eta_2, \tag{71}$$

where the reduced-rank SINR is given by

$$\xi_r = \frac{|\alpha|^2}{\sigma_d^2 - \mathbf{r}_{zd} \mathbf{R}_z^{-1} \mathbf{r}_{zd}}. \tag{72}$$

The probability of detection of this new reduced-rank AMF test in (71) is modified to

$$P_{D_r} = \sum_{n=0}^{\infty} \left(\frac{(\xi_r)^n e^{-\xi_r}}{n!} \right) Q\left(n+1, \eta_2\right), \tag{73}$$

and the probability of false alarm retains the form,

$$P_{FA} = Q\left(1, \eta_2\right) = e^{-\eta_2}. \tag{74}$$

Note that the expressions in (69), (70), (71), (72), (73) and (74) are valid for any unitary operator used for rank reduction with a subspace selection rule which chooses M of the N columns of the unitary operator. This includes, but is not limited to the reduced-rank principal component and cross-spectral AMF CFAR tests, which use the unitary matrix composed of the eigenvectors of $\mathbf{R}_b$.

The reduced-rank AMF CFAR test is now examined for the case of unknown covariance. The standard approach for radar detection when the noise covariance is unknown is to obtain an estimate

from some $L > KJ$ range gates in the neighborhood of the range gate currently being tested for signal presence. The data in the range gate of interest is termed the primary data. The L nearby range gates, which yield what is termed the secondary or auxillary data, are assumed to be target-free. It is also possible to assume that only multiple snapshots of the same range gate are available. The presentation of the material in this section follows similar derivations given previously for full-rank detectors [26, 27, 24, 25, 28, 29, 30].

It is well known that the maximum likelihood estimate of the covariance matrix $\mathbf{R}$ is provided by the sample covariance matrix $\hat{\mathbf{R}}$, i.e.

$$\hat{\mathbf{R}} = \frac{1}{L}\sum_{i=1}^{L} \mathbf{n}_i \mathbf{n}_i^H, \tag{75}$$

where $\mathbf{n}_i$ is the $KJ \times 1$ vector of samples from the i-th nearby range gate. Define an auxillary $KJ \times L$ data matrix $\mathbf{A}$ by

$$\mathbf{A} = [\mathbf{n}_1, \quad \mathbf{n}_2, \quad \cdots \quad \mathbf{n}_L], \tag{76}$$

so that the sample covariance matrix $\hat{\mathbf{R}}$ may be written in the form,

$$\hat{\mathbf{R}} = \frac{1}{L}\mathbf{A}\mathbf{A}^H. \tag{77}$$

Then the AMF CFAR test is expressed in terms of the sample covariance matrix as follows:

$$\Lambda_{2s} = \frac{\left|\mathbf{s}^H \hat{\mathbf{R}}^{-1}\mathbf{x}\right|^2}{\mathbf{s}^H \hat{\mathbf{R}}^{-1}\mathbf{s}} = \frac{L\left|\mathbf{s}^H \left(\mathbf{A}\mathbf{A}^H\right)^{-1}\mathbf{x}\right|^2}{\mathbf{s}^H \left(\mathbf{A}\mathbf{A}^H\right)^{-1}\mathbf{s}} \underset{H_0}{\overset{H_1}{\gtrless}} \eta_2. \tag{78}$$

The data matrix $\mathbf{A}$ is expressed now in the form

$$\mathbf{A} = \mathbf{R}^{1/2}\boldsymbol{X}, \tag{79}$$

where $\boldsymbol{X}$ is a $KJ \times L$ matrix of zero-mean, independent and identically distributed, complex Gaussian variates with unit variance. Then an equivalent test to the sampled data AMF CFAR

test in (78) is provided by

$$\Lambda_{2_s} = \frac{L\left|\mathbf{s}^H\left(\boldsymbol{X}\boldsymbol{X}^H\right)^{-1}\mathbf{x}\right|^2}{\mathbf{s}^H\left(\boldsymbol{X}\boldsymbol{X}^H\right)^{-1}\mathbf{s}} \underset{H_0}{\overset{H_1}{\gtrless}} \eta_2. \tag{80}$$

The methodology used in the previous section for transforming the observed data into the GSC form is now applied to the auxillary data. The matrix $\mathbf{T}$ defined in (31) operates on the data matrix $\boldsymbol{X}$ defined in (79). The transformed data matrix $\tilde{\boldsymbol{X}}$ has the form,

$$\tilde{\boldsymbol{X}} = \mathbf{T}\boldsymbol{X} = \begin{bmatrix} \boldsymbol{\mathcal{D}} \\ \boldsymbol{\mathcal{B}} \end{bmatrix}, \tag{81}$$

where $\boldsymbol{\mathcal{D}}$ is the $1 \times L$ beamformed data vector and $\boldsymbol{\mathcal{B}}$ is the $N \times L$ noise subspace data matrix where $N = KJ - 1$.

The rank reducing $N \times M$ transform $\boldsymbol{\mathcal{U}}$, defined to be composed of those M eigenvectors of $\mathbf{R}_b$ which maximize the cross-spectral metric given in (65), is applied next to form a $(M+1)\times(M+1)$ transformed reduced-rank sample covariance matrix as follows:

$$\hat{\mathbf{R}}_{\tilde{X}} = \begin{bmatrix} 1 & \mathbf{0}^H \\ \mathbf{0} & \boldsymbol{\mathcal{U}}^H \end{bmatrix} \mathbf{T}\boldsymbol{X}\boldsymbol{X}^H\mathbf{T}^H \begin{bmatrix} 1 & \mathbf{0}^H \\ \mathbf{0} & \boldsymbol{\mathcal{U}}^H \end{bmatrix}^H = \begin{bmatrix} \boldsymbol{\mathcal{D}}\boldsymbol{\mathcal{D}}^H & \boldsymbol{\mathcal{D}}\boldsymbol{\mathcal{Z}}^H \\ \boldsymbol{\mathcal{Z}}\boldsymbol{\mathcal{D}}^H & \boldsymbol{\mathcal{Z}}\boldsymbol{\mathcal{Z}}^H \end{bmatrix} = \begin{bmatrix} \hat{\sigma}_d^2 & \hat{\mathbf{r}}_{zd}^H \\ \hat{\mathbf{r}}_{zd} & \hat{\mathbf{R}}_z \end{bmatrix}, \tag{82}$$

where the reduced-rank $M \times L$-dimensional auxillary data vector $\boldsymbol{\mathcal{Z}}$ is given by

$$\boldsymbol{\mathcal{Z}} = \boldsymbol{\mathcal{U}}^H\boldsymbol{\mathcal{B}}. \tag{83}$$

The optimal $(M+1)\times 1$-dimensional reduced-rank weight vector in these transformed coordinates is given by

$$\hat{\mathbf{w}}_{gsc} = \begin{bmatrix} 1 \\ -\hat{\mathbf{w}}_r \end{bmatrix}, \tag{84}$$

where the $M \times 1$-dimensional vector $\hat{\mathbf{w}}_r$ is provided by the Wiener solution corresponding to the filter depicted in Figure 4, namely

$$\hat{\mathbf{w}}_r = \left(\boldsymbol{\mathcal{Z}}\boldsymbol{\mathcal{Z}}^H\right)^{-1}\boldsymbol{\mathcal{Z}}\boldsymbol{\mathcal{D}}^H = \hat{\mathbf{R}}_z^{-1}\hat{\mathbf{r}}_{zd}. \tag{85}$$

The resulting output power is given by

$$\hat{P}_r = \hat{\sigma}_d^2 - \hat{\mathbf{r}}_{zd}^H \hat{\mathbf{R}}_z^{-1} \hat{\mathbf{r}}_{zd}. \tag{86}$$

The primary data is also transformed by $\mathbf{R}^{-1/2}$ and $\mathbf{T}$ to obtain

$$\mathbf{x}_p = \mathbf{T}\mathbf{R}^{-1/2}\mathbf{x} = \begin{bmatrix} d \\ \mathbf{b} \end{bmatrix}, \tag{87}$$

and the reduced-rank $M \times 1$-dimensional primary data vector is then given by

$$\mathbf{z}_p = \mathcal{U}^H \mathbf{b}. \tag{88}$$

The reduced-rank AMF CFAR test with an unknown covariance corresponding to the test in (78) is expressed now in the form,

$$\Lambda_{2_{s_r}} = \frac{\left| d - \hat{\mathbf{w}}_r^H \mathbf{z}_p \right|^2}{\hat{\sigma}_d^2 - \hat{\mathbf{r}}_{zd}^H \hat{\mathbf{R}}_z^{-1} \hat{\mathbf{r}}_{zd}} = \frac{|y_r|^2}{\hat{P}_r} \underset{H_0}{\overset{H_1}{\gtrless}} \eta_{2_s}, \tag{89}$$

where the threshold η_{2_s} in (89) is related to the original threshold η_2 in (78) by

$$\eta_{2_s} = \frac{\eta_2}{L}. \tag{90}$$

Next the denominator of the reduced-rank sampled data AMF CFAR test in (89) is rewritten in the form,

$$\hat{P}_r = \mathcal{D}\left(\mathbf{I} - \mathcal{Z}^H \hat{\mathbf{R}}_z^{-1} \mathcal{Z}\right) \mathcal{D}^H = \mathcal{D}\mathbf{C}\mathcal{D}^H. \tag{91}$$

The vector $\mathcal{D}$ is a $1 \times L$ zero-mean, white Gaussian random vector. Therefore the distribution of $\mathcal{D}$ can be denoted by

$$\mathcal{D} \longleftrightarrow N_L(\mathbf{0}, \mathbf{I}), \tag{92}$$

where $N_L(\mathbf{0}, \mathbf{I})$ is a joint Gaussian density of zero mean and covariance $\mathbf{I}$, the $L \times L$ identity matrix. Also it is easily shown by (83) that the matrix $\mathbf{I} - \mathbf{C}$, given by

$$(\mathbf{I} - \mathbf{C}) = \mathcal{Z}^H \hat{\mathbf{R}}_z^{-1} \mathcal{Z} \tag{93}$$

is a projection matrix of rank M which projects vectors onto the reduced-rank auxillary data noise subspace. The matrix $\mathbf{C}$ is also an idempotent projection matrix of rank $L-M$, and the distribution of $\hat{P}_r$ is therefore central χ^2 with $L-M$ degrees of freedom [31, Theorem 1.4.2, p.27]. Thus the distribution of $\hat{P}_r$ is expressed by

$$\hat{P}_r \longleftrightarrow \chi^2_{L-M}. \tag{94}$$

The output of the reduced-rank GSC form array variate may be expressed next by

$$y_r = d - \hat{\mathbf{r}}_{zd}^H \hat{\mathbf{R}}_z^{-1} \mathbf{z}_p, \tag{95}$$

which is conditionally complex Gaussian distributed when the quantities $\mathbf{z}_p$ and $\boldsymbol{\mathcal{Z}}$ are fixed. The conditional covariance of y_r is ρ^{-1}, where ρ is given by

$$\rho = \frac{1}{1 + \mathbf{z}_p^H \hat{\mathbf{R}}_z^{-1} \mathbf{z}_p}. \tag{96}$$

The parameter ρ is the well known RMB loss factor [4, 32, 25, 26] for the reduced-rank processor, and it has a central Beta distribution which is given by

$$f_\rho(\rho) = \frac{\rho^{L-M}(1-\rho)^{M-1}}{\beta(M, L-M+1)}, \tag{97}$$

where

$$\beta(a,b) = \frac{(a-1)!\,(b-1)!}{(a+b-1)!}. \tag{98}$$

Hence the distribution of the reduced-rank AMF CFAR test is given by

$$\Lambda_{2s_r}(y_r, \hat{P}_{n_r} | \mathbf{z}_p, \boldsymbol{\mathcal{Z}}) \longleftrightarrow \rho^{-1} \frac{\chi^2(\delta)}{\chi^2_{L-M}} = \frac{\gamma}{\rho}, \tag{99}$$

where δ is the noncentrality parameter, given by

$$\delta = \rho \xi_r. \tag{100}$$

The parameter γ is the ratio of two independent χ^2 variables where the numerator is noncentral χ^2 distributed. Hence, under hypothesis H_1, γ has a noncentral F distribution [31, Theorem 1.3.6, p.24] given by

$$f_{\gamma|\rho,H_1}(\gamma) = \frac{e^{-\delta}}{\beta(1, L-M)\,(1+\gamma)^{L-M+1}}\ {}_1F_1\left(L-M+1, 1, \frac{\delta\,\gamma}{1+\gamma}\right). \tag{101}$$

Therefore, the conditional distribution of the test $\Lambda_{2_{s_r}}$ given $\boldsymbol{z}_p$ and $\boldsymbol{\mathcal{Z}}$ under hypothesis H_1, may be expressed by

$$f_{\Lambda_{2_{s_r}}|\rho,H_1}(q) = \frac{e^{-\delta}}{\beta(1, L-M)}\,\frac{\rho}{(1+q\rho)^{L-M+1}}\ {}_1F_1\left(L-M+1, 1, \frac{\delta\,q\,\rho}{1+q\rho}\right). \tag{102}$$

The unconditional probability density function of the reduced-rank AMF CFAR test is then computed as follows:

$$f_{\Lambda_{2_{s_r}}|H_1}(q) = \int_0^1 f_{\Lambda_{2_{s_r}}|\rho,H_1}(q)\, f_{\rho|H_1}(\rho)\, d\rho, \tag{103}$$

which is expressible in the form,

$$f_{\Lambda_{2_{s_r}}|H_1}(q) = \frac{1}{\beta(1, L-M)\,\beta(M, L-M+1)} \int_0^1 e^{-\delta}\,\frac{\rho^{L-M+1}\,(1-\rho)^{M-1}}{(1+q\rho)^{L-M+1}}\,{}_1F_1\left(L-M+1, 1, \frac{\delta\,q\,\rho}{1+q\rho}\right) d\rho, \tag{104}$$

where $q \geq 0$. Finally by (104) for a fixed threshold η, the probability of detection is computed to be

$$P_D(\eta) = \int_\eta^\infty f_{\Lambda_{2_{s_r}}|H_1}(q)\, dq, \tag{105}$$

which when evaluated has the form

$$P_D(\eta) = \int_0^1 \frac{e^{-\delta}\,\rho^{L-M}\,(1-\rho)^{M-1}}{\beta(1, L-M)\,\beta(M, L-M+1)} \int_{\frac{\eta\rho}{1+\eta\rho}} (1-q)^{L-M-1}\ {}_1F_1\left(L-M+1, 1, \delta q\right) dq\, d\rho. \tag{106}$$

The distribution of the reduced-rank AMF CFAR test under hypothesis H_0 requires that the variable δ be set to zero, and (104) reduces to

$$f_{\Lambda_{2_{SR}}|H_0}(q) = \frac{1}{\beta(1, L-M)\,\beta(M, L-M+1)} \int_0^1 \frac{\rho^{L-M+1}\,(1-\rho)^{M-1}}{(1+q\rho)^{L-M+1}}\, d\rho, \tag{107}$$

which, for the selected threshold η, yields a false alarm probability given by

$$P_{FA}(\eta) = \int_\eta^\infty f_{\Lambda_{2_{SR}}|H_0}(q)\, dq = \frac{1}{\beta(1, L-M)\,\beta(M, L-M+1)} \int_\eta^\infty \int_0^1 \frac{\rho^{L-M+1}\,(1-\rho)^{M-1}}{(1+q\rho)^{L-M+1}}\, d\rho dq. \tag{108}$$

Since the P_{FA} is only a function of the threshold η and the integers L and M, all of which are held fixed, the test $\Lambda_{2_{SR}}$ has a constant false alarm rate.

7 An Example of the Performance of Partially Adaptive Radar

A simulation is now considered which utilizes the parameters of the ARPA Mountain Top radar in order to compare the performance of the reduced-rank detectors to that of the full-rank, joint domain optimal detector. The AMF CFAR test with known covariance is utilized exclusively for this example.

The Mountain Top radar employs the Radar Surveillance Technology Experimental Radar (RSTER) and the Inverse Displaced Phase Center Array (IDPCA), co-located at the same site [33]. It is assumed that the radar is in the RSTER-90 configuration and the receive-only mode. The transmit frequency is 450 MHz. This radar consists of K=14 elements and J=16 pulses in the PRI. The elevation angle θ is fixed (pre-beamformed), and the azimuth angle ϕ is the only free parameter. The dimension of the adaptive processor is $KJ = 224$. The GSC processor beamforms the target signal in one branch and, using a bloching matrix $\mathbf{B}$, blocks the target signal from the other branch. The noise subspace data vector is then of dimension $N = KJ - 1 = 223$. The corresponding full-rank GSC weight vector is also of dimension 223×1.

For the purposes of this analysis, three barrage jammers and land clutter compose the interference enviroment and one target signal is present. It is assumed that the radar platform is at a height of 500 meters, and that the platform velocity is 500 meters per second. The target, which is also at a height of 500 meters, has a range of 22 kilometers and an azimuth of $-30°$. The target velocity is 250 meters per second. This target has a signal-to-noise ratio (SNR) of 15 dB, representing a small, non-fluctuating, constant radar cross-section target. The three jammers have azimuth angles of $-60°$, $30°$ and $60°$, with jammer-to-noise ratios of 30 dB, 40 dB, and 30 dB, respectively. The clutter-to-noise ratio is set to be 30 dB.

The cross-spectral metric is now applied to the GSC and the detection performance is compared to the principal component techniques such as PCI [13, 14], which has also been termed an eigen-canceler [12, 15]. The performance of the fully adaptive GSC, the partially adaptive eigen-subspace GSC, and the partially adaptive cross-spectral subspace GSC processors are evaluated.

To obtain the performance of the subspace selection techniques, let the dimension of the adaptive processor be reduced from $N = 223$ weights to $M = 50$. The dimension of the noise subspace eigenstructure is calculated to be approximately 70. This is the lower bound for the standard rank reduction techniques [9, 10, 11]. The power spectrum of the data, averaged over 500 snapshots, is presented in Figure 7, from which it is evident that the target signal is not discernible. Figure 8 presents the gain of the full-rank spatio-temporal Wiener filter, from which it is seen that the optimal space-time weight vector of dimension 223 is capable of attenuating all jammers and clutter while passing the target signal. The full-rank Wiener filter SINR is 38.28 dB. Figure 9 depicts the spatio-temporal gain of the rank 50 eigen-subspace Wiener filter. The clutter and most of the power from the three jammers is passed with relatively high gain; there is little attenuation of the noise.

The output SINR for the eigen-subspace Wiener filter is 25.98 dB, reflecting a loss of 12.3 dB. The spatio-temporal gain of the rank 50 cross-spectral subspace Wiener filter is depicted in Figure 10. It can be seen that by simply selecting a different set of 50 eigenvectors, the resulting array response closely approximates the full-rank optimal STAP matched filter and the clutter and jammers are attenuated. The resulting output SINR is 28.03 dB, reflecting a loss of only 0.25 dB in reducing the rank from 223 to 50.

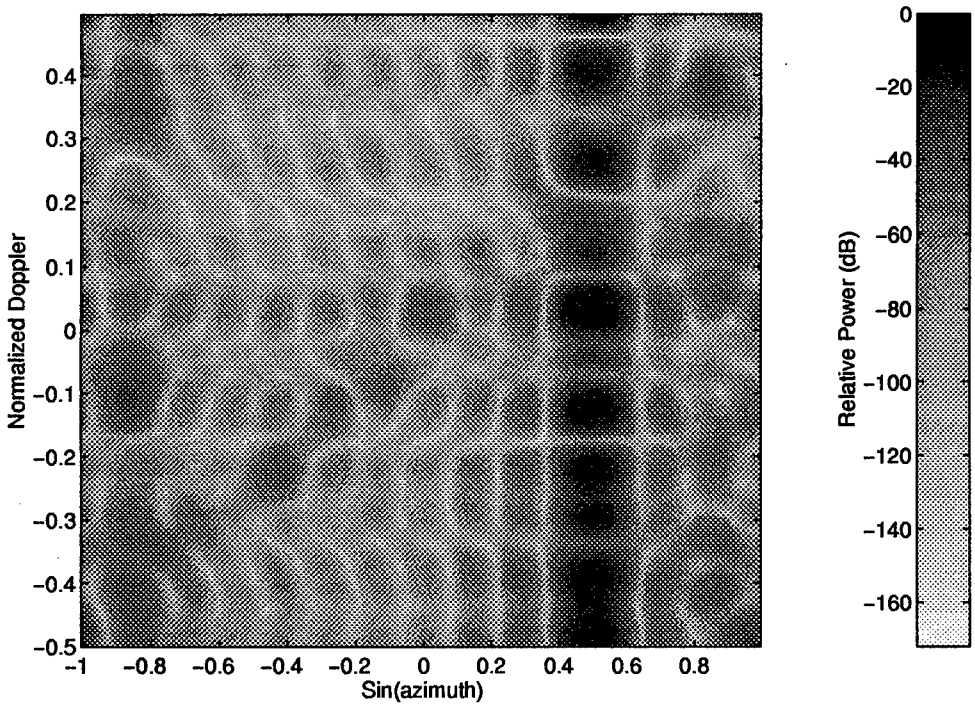

Figure 7: The power spectrum of the data.

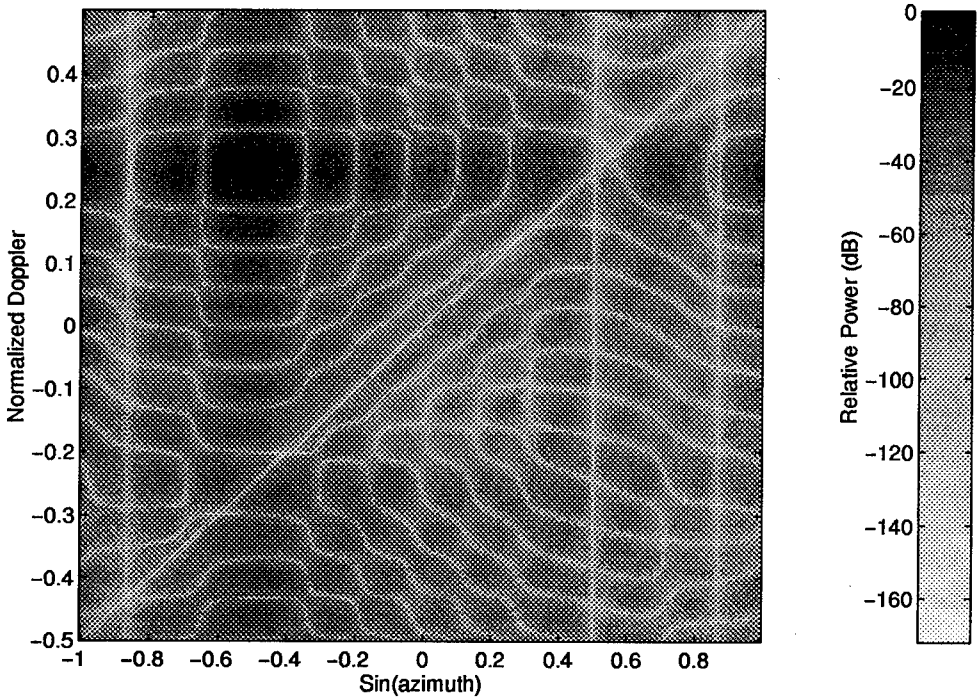

Figure 8: The full-rank Wiener filter.

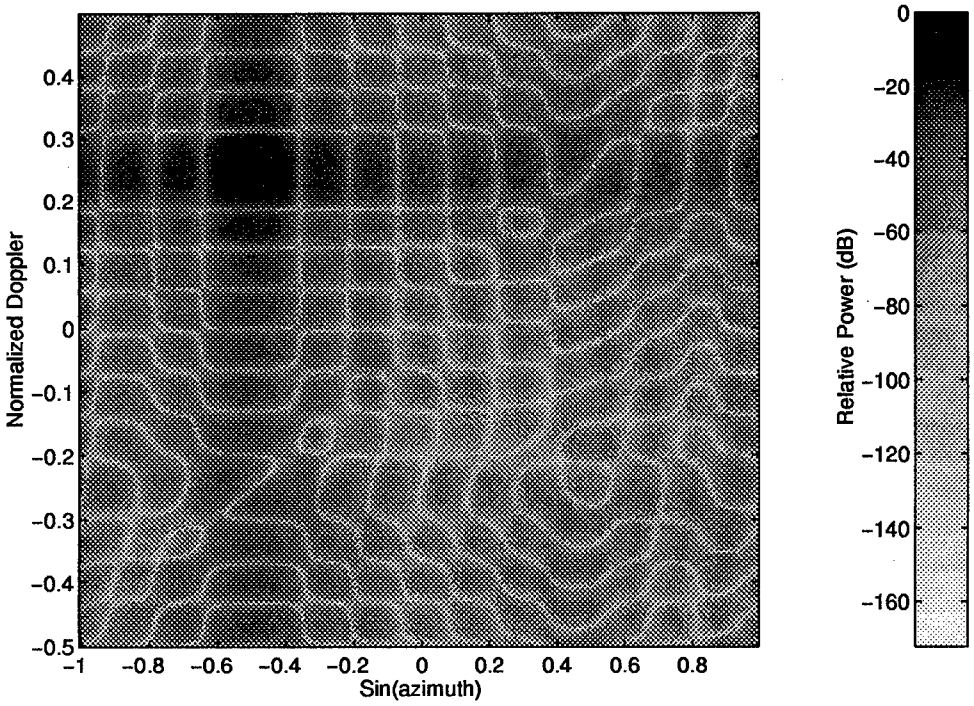

Figure 9: The reduced-rank eigen-subspace Wiener filter.

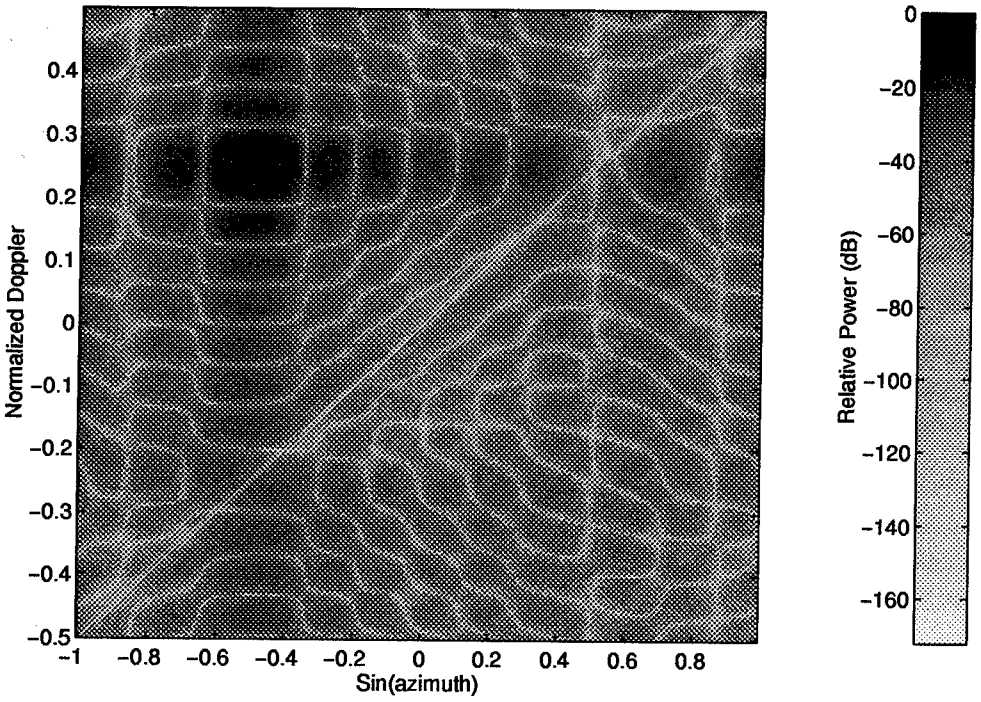

Figure 10: The reduced-rank cross-spectral subspace Wiener filter.

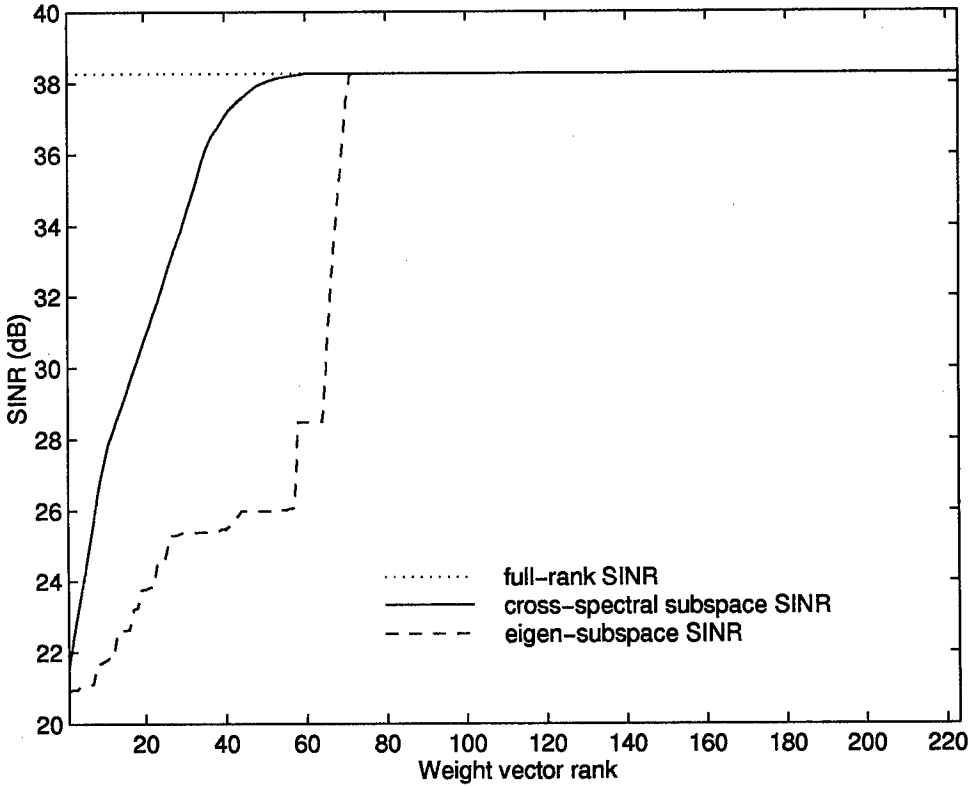

Figure 11: The output SINR of the reduced-rank processors as a function of the rank of the data.

The performance of these two reduced-rank processors may also be evaluated by plotting the output SINR as a function of Wiener filter rank. The SINR for the eigen-subspace and cross-spectral subspace reduced-rank processors are compared to the full-rank SINR in Figure 11 as the rank increases from 1 to 223. It can be seen from this figure that the eigen-subspace processor converges to the optimal SINR in an abrupt manner, thereby obtaining the optimal value only once the Wiener filter rank reaches the dimension of the noise subspace eigenstructure. This is characteristic of the eigen-subspace techniques in nearly all of its applications since the principal components method does not yield an optimal filter as a function of rank. By contrast the cross-spectral metric depicts an exponential-like convergence to the optimal SINR.

The above simulation shows that the reduced-rank Wiener filter in the cross-spectral subspace outperforms the Wiener filter in the eigen-subspace for all filter ranks less than the dimension of the noise subspace eigenstructure. It is verified in Figure 11 that the cross-spectral metric provides an upper-bound to the SINR performance achievable by a reduction of the number of eigenvectors of the array covariance matrix. Finally, note for the Mountain Top radar example that the reduction of the rank to 50 weights can be interpreted as an error in estimating the dimension of the noise subspace eigenstructure. It is clear from Figure 11 that the penalty in SINR performance for underestimating the rank of the noise subspace eigenstructure is greatly reduced in the cross-spectral approach to rank reduction. This robustness property is paramount for reduced-rank detection in unknown noise environments.

Next the probability of false alarm for each test is set to $P_{FA} = 10^{-6}$. The detection probabilities are calculated for the full-rank test (223 adaptive weights) and for the two reduced-rank tests (50 adaptive weights) in the eigen-subspace and the cross-spectral subspace. The resulting plots of P_D versus the normalized output SINR are presented in Figure 12. The normalized SINR is

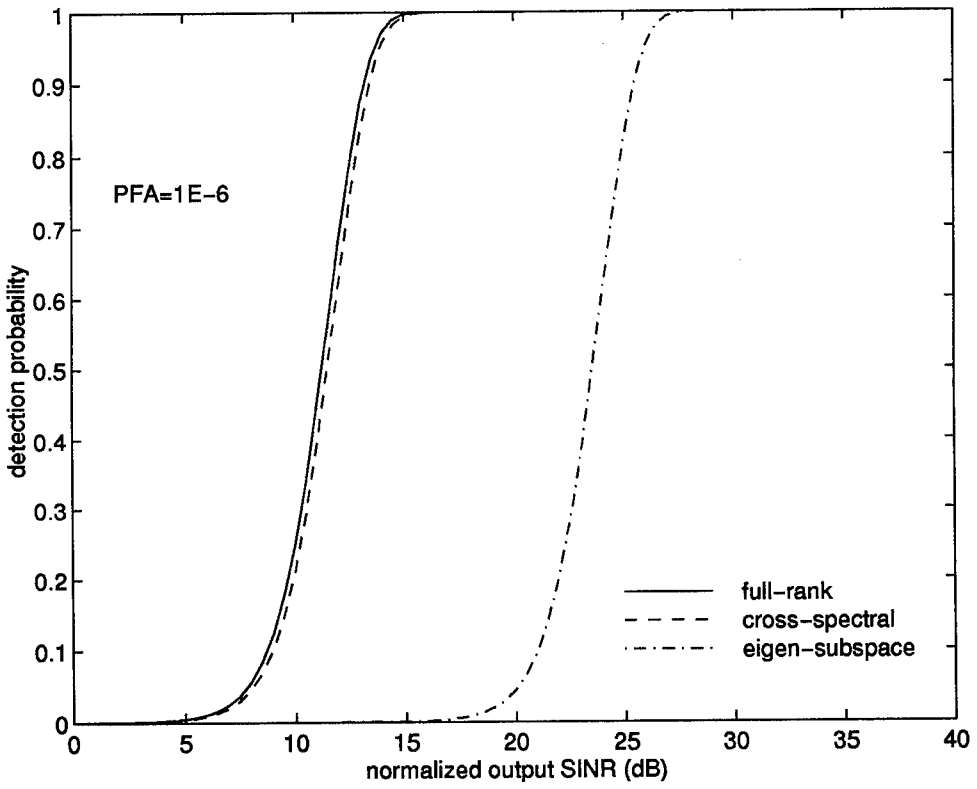

Figure 12: The AMF probability of detection versus normalized output SINR.

calculated by dividing the output SINR of each reduced-rank detector by the output SINR of the full-rank detector. It is seen that the full-rank AMF detector and the rank 50 cross-spectral AMF detector demonstrate very similar performance. By comparison, the rank 50 eigen-subspace detector performs quite poorly. Recall that a target input SNR of 15 dB is used in the graphical examples presented earlier in this section. The full-rank and cross-spectral AMF detectors both yield a detection probability nearly equal to unity for this target. The eigen-subspace detector, however, yields a P_D near zero for this same scenario. The rank 50 cross-spectral subspace detector yields a 12 dB improvement in detection sensitivity over the rank 50 eigen-subspace detector. This corresponds to the estimated 12 dB gain of the cross-spectral subspace processor over the SINR obtainable by the eigen-subspace processor at rank 50 as it is depicted in Figure 11.

8 Conclusions

In this report a general methodology is introduced in order to describe reduced-rank detectors and to analyze their statistical properties and performance. Although the AMF CFAR test is emphasized in this report, the analysis technique developed herein may be extended readily to nearly any other test by simply relating the variables which compose the test to the GSC. For example, the generalized likelihood ratio test (GLRT) [23], now denoted Λ_3, results in another CFAR test which takes the form

$$\Lambda_3 = \frac{1+\mathbf{x}^H\mathbf{R}^{-1}\mathbf{x}}{1+\mathbf{x}^H\mathbf{R}^{-1}\mathbf{x}-\frac{|\mathbf{s}^H\mathbf{R}^{-1}\mathbf{x}|^2}{\mathbf{s}^H\mathbf{R}^{-1}\mathbf{s}}} = 1+\frac{|y|^2}{P\left(1+\mathbf{b}^H\mathbf{R}_b^{-1}\mathbf{b}\right)} \underset{H_0}{\overset{H_1}{\gtrless}} \eta_3. \tag{109}$$

For this case the reduced-rank GLRT is expressed in the form,

$$\Lambda_{3_r} = 1+\frac{|v_r|^2}{P_r} \underset{H_0}{\overset{H_1}{\gtrless}} \gamma_3, \tag{110}$$

where the term $v_r = \sqrt{\rho}y_r$ and ρ is the reduced-rank RMB loss factor in (96).

The computational complexity requirements of the eigendecomposition performed for subspace selection suggest that other procedures need to be discussed. It is noted that other unitary operators $\mathbf{U}$ may be used with the cross-spectral metric to determine the transformation $\boldsymbol{\mathcal{U}}$, to yield new reduced-rank tests which may approximately exhibit the optimal performance obtained herein. The Gram-Schmidt procedure is one example of a lower-complexity transformation which can result in excellent performance with the cross-spectral metric. Another example is the approximation of the cross-spectral metric which uses a unitary operator that does not completely decorrelate the noise subspace covariance matrix. This technique is used in [19], where the DCT matrix was used in order to reduce the computational complexity.

Finally, it is possible to form new detectors by incorporating other constraints in conjuction with the STAP detection linear constraint. Examples of this include derivative constraints [34] and

other additional linear constraints which take advantage of any available a priori knowledge of the interference environment [35, 36]. Fixed transformations of the data prior to adaptive filtering also belong to this category and the popular element-space pre-Doppler and post-Doppler algorithms, as well as their beamspace analogies, may be formulated in the context provided by this report.

Appendix: Algorithms for Finding an Orthonormal Signal Blocking Matrix B

In this appendix, two simple algorithms are described to determine an orthonormal signal blocking matrix $\mathbf{B}$ given the normalized $N \times 1$ dimensional steering vector $\mathbf{s}$. The first algorithm is more accurate and utilizes the singular value decomposition (SVD). The second algorithm is faster, and uses the QR decomposition. Both of these algorithms are derived and explained in detail in many linear and numerical algebra texts, such as [37].

Algorithm 1

$$\boxed{\begin{array}{l}[\mathbf{U}, \mathbf{S}, \mathbf{V}] = \text{svd}(\mathbf{s}^T) \\ \mathbf{B} = \mathbf{V}(:, 2:N)\end{array}}$$

Algorithm 2

$$\boxed{\begin{array}{l}[\mathbf{Q}, \mathbf{R}] = \text{qr}(\mathbf{s}) \\ \mathbf{B} = \mathbf{Q}^H(:, 2:N)\end{array}}$$

In many cases, a non-orthonormal signal blocking matrix may be easily constructed and the Gram-Schmidt proceedure can be implemented to provide the orthonormalization. One example of this is a system which utilizes a primary space-time steering vector to set the array manifold in angle and Doppler. The normalized steering vector $\mathbf{s}$ is then fixed to point broadside with respect to the array. The non-orthonormal signal blocking matrix, under these conditions, is implemented by simply taking the difference of the appropriate input signals. This is identical to the array configuration presented in [2] for narrowband arrays.

References

[1] S.P. Applebaum. Adaptive arrays. Technical Report SPL TR 66-1, Syracuse University Research Corporation, August 1966.

[2] S.P. Applebaum and D.J. Chapman. Adaptive arrays with main beam constraints. *IEEE Trans. Antenn. Propagat.*, AP-24(5):650–662, September 1976.

[3] L.E. Brennan and I.S. Reed. Theory of adaptive radar. *IEEE Trans. Aerosp. Electron. Syst.*, 9:237–251, March 1973.

[4] I.S. Reed, J.D. Mallett, and L.E. Brennan. Rapid convergence rate in adaptive arrays. *IEEE Trans. Aerosp. Electron. Syst.*, AES-10(6):853–863, November 1974.

[5] S.C. Liu and L.W. Nolte. Performance evaluation of array processors for detecting Gaussian signals. *IEEE Trans. Acoust., Speech, Signal Processing*, 28:328–333, June 1980.

[6] L.W. Brooks and I.S. Reed. Equivalence of the likelihood ratio processor, the maximum signal-to-noise ratio filter and the Wiener filter. *IEEE Trans. Aerosp. Electron. Syst.*, AES-8:690–692, September 1972.

[7] L.L. Scharf. *Statistical Signal Processing.* Addison-Wesley, Reading, MA, 1991.

[8] O.L. Frost. An algorithm for linearly constrained adaptive array processing. *Proc. IEEE*, 60(8):926–935, August 1972.

[9] W.F. Gabriel. Using spectral estimation techniques in adaptive processing antenna systems. *IEEE Trans. Antenn. Propagat.*, AP-34(3):291–300, March 1986.

[10] N.L. Owsley. Sonar array processing. In S. Haykin, editor, *Array Signal Processing*, chapter 3. Addison-Wesley, Reading, MA, 1991.

[11] B.D. Van Veen. Eigenstructure based partially adaptive array design. *IEEE Trans. Antenn. Propagat.*, 36(3):357–362, March 1988.

[12] A.M. Haimovich and Y. Bar Ness. An eigenanalysis interference canceler. *IEEE Trans. Signal Processing*, 39(1):76–84, January 1991.

[13] I.P. Kirsteins and D.W. Tufts. Adaptive detection using a low rank approximation to a data matrix. *IEEE Trans. Aerosp. Electron. Syst.*, 30(1):55–67, January 1994.

[14] W. Harrison and D. Tufts. Rapidly adaptive mainbeam jammer nulling. In *Proc. ASAP Workshop*, volume ASAP-3 Addendum. MIT Lincoln Laboratory, July 1994.

[15] A. Haimovich, M. Berlin, and X. Wu. Performance of the eigencanceler: Eigenanalysis space-time adaptive radar. In *Proc. ASAP Workshop*, volume ASAP-3, pages 419–445. MIT Lincoln Laboratory, April 1995.

[16] H. Hotelling. *Analysis of a Complex of Statistical Variables into Principal Components.* Warwick and York, Baltimore, MD, 1933.

[17] C. Eckart and G. Young. The approximation of one matrix by another of lower rank. *Psychometrica*, 1:211–218, 1936.

[18] J.S. Goldstein and I.S. Reed. Subspace selection for partially adaptive sensor array processing. *IEEE Trans. on Aerosp. Electron. Syst.*, Accepted for publication, 1996.

[19] J.S. Goldstein and I.S. Reed. Reduced rank adaptive filtering. *IEEE Trans. Signal Processing*, Accepted for publication, 1996.

[20] J.S. Goldstein and I.S. Reed. Performance measures for optimal constrained beamformers. *IEEE Trans. Antenn. Propagat.*, Accepted for publication, 1996.

[21] L.J. Griffiths and C.W. Jim. An alternative approach to linearly constrained adaptive beamforming. *IEEE Trans. Antenn. Propagat.*, AP-30(1):27–34, January 1982.

[22] J. Ward. Space-time adaptive processing for airborne radar. Technical Report 1015, MIT Lincoln Laboratory, December 1994.

[23] E.J. Kelly. An adaptive detection algorithm. *IEEE Trans. Aerosp. Electron. Syst.*, 23:115–127, November 1986.

[24] W.S. Chen and I.S. Reed. A new CFAR detection test for radar. *Digital Signal Proc.*, 4:198–214, October 1991.

[25] F.C. Robey, D.R. Fuhrmann, E.J. Kelly, and R. Nitzberg. A CFAR adaptive matched filter detector. *IEEE Trans. Aerosp. Electron. Syst.*, 28(1):208–216, January 1992.

[26] X. Yu and I.S. Reed. Adaptive detection of signals with linear feature mappings and representations. *IEEE Trans. Signal Processing*, 43(12):2953–2963, December 1995.

[27] I.S. Reed, Y.L. Gau, and T.K. Truong. A simultaneous CFAR detection and ML estimation STAP algorithm for airborne radar. *IEEE Trans. on Aerosp. Electron. Syst.*, Submitted for publication, 1995.

[28] E.J. Kelly. Adaptive detection in non-stationary interference, part I and part II. Technical Report TR-724, MIT Lincoln Laboratory, June 1985.

[29] P. Monticciolo. Adaptive detection in stationary and nonstationary noise environments. Technical Report TR-937, MIT Lincoln Laboratory, February 1994.

[30] A. Steinhardt. Adaptive multisensor detection and estimation. In S. Haykin and A. Steinhardt, editors, *Adaptive Radar Detection and Estimation*, chapter 3. John Wiley and Sons, New York, NY, 1992.

[31] R.J. Muirhead. *Aspects of Multivariate Statistical Theory.* John Wiley & Sons, New York, NY, 1982.

[32] E.J. Kelly. Adaptive detection in non-stationary interference, part III. Technical Report TR-761, MIT Lincoln Laboratory, August 1987.

[33] G.W. Titi. An overview of the ARPA/Navy Mountaintop Program. In *Proc. of the IEEE Adapt. Ant. Systems Symp.*, Long Island, NY, November 1994.

[34] K.M. Buckley and L.J. Griffiths. An adaptive generalized sidelobe canceller with derivative constraints. *IEEE Trans. Antenn. Propagat.*, AP-34:311–319, March 1986.

[35] B.D. Van Veen and R.A. Roberts. Partially adaptive beamformer design via output power minimization. *IEEE Trans. Acoust., Speech, Signal Processing*, ASSP-35(11):1524–1532, November 1987.

[36] B.D. Van Veen. Minimum variance beamforming. In S. Haykin and A. Steinhardt, editors, *Adaptive Radar Detection and Estimation*, chapter 4. John Wiley and Sons, New York, NY, 1992.

[37] G. Strang. *Linear Algebra and its Applications.* Harcourt Brace Jovanovich, Inc, San Diego, CA., 1988.

*U.S. GOVERNMENT PRINTING OFFICE: 1997-509-127-47141

MISSION

OF

ROME LABORATORY

Mission. The mission of Rome Laboratory is to advance the science and technologies of command, control, communications and intelligence and to transition them into systems to meet customer needs. To achieve this, Rome Lab:

a. Conducts vigorous research, development and test programs in all applicable technologies;

b. Transitions technology to current and future systems to improve operational capability, readiness, and supportability;

c. Provides a full range of technical support to Air Force Materiel Command product centers and other Air Force organizations;

d. Promotes transfer of technology to the private sector;

e. Maintains leading edge technological expertise in the areas of surveillance, communications, command and control, intelligence, reliability science, electro-magnetic technology, photonics, signal processing, and computational science.

The thrust areas of technical competence include: Surveillance, Communications, Command and Control, Intelligence, Signal Processing, Computer Science and Technology, Electromagnetic Technology, Photonics and Reliability Sciences.